Chapter 14

Analysis of Biomolecules Using Surface Plasmons

M. Willander and Safaa Al-Hilli

Summary

Surface plasmon resonance (SPR) biosensors are optical sensors that use special electromagnetic waves (surface plasmon-polaritons) to probe interactions between an analyte in solution and a biomolecular recognition element immobilized on the SPR sensor surface. Major application areas include the detection of biological analytes and analysis of biomolecular interactions, where SPR biosensors provide benefits of label-free real-time analytical technology. The information obtained is both qualitative and quantitative and it is possible to obtain the kinetic parameters of the interaction. This new technology has been used to study a diverse set of interaction partners of biological interest, such as protein–protein, protein–lipids, protein–nucleic acids, or protein and low molecular weight molecules such as drugs, substrates, and cofactors. In addition to basic biomedical research, the SPR biosensor has recently been used in food analysis, proteomics, immunogenicity, and drug discovery. This chapter reviews the major developments in SPR technology. The main application areas are outlined and examples of applications of SPR sensor technology are presented. Future prospects of SPR sensor technology are discussed.

Key words: Surface plasmons resonance, Biosensors, Optical sensor, Biomolecular interaction

1. Introduction

Surface plasmons (SPs) are of interest to a wide spectrum of scientists ranging from physicists, chemists, and material scientists to biologists. Renewed interest in SPs comes from recent advances that allow metals to be structured and characterized on the nanometer scale. In turn, this has enabled us to control SP properties to reveal new aspects of their underlying science and tailor them for specific applications.

SPs were widely recognized in the field of surface science following the pioneering work of Ritchie in the 1950s *(1)*. SPs are waves that propagate along the surface of a conductor, usually a

James Weifu Lee and Robert S. Foote (eds.), *Micro and Nano Technologies in Bioanalysis*,
Methods in Molecular Biology, vol. 544
DOI 10.1007/978-1-59745-483-4_14,

metal. These are essentially light waves that are trapped on the surface because of their interaction with free electrons of the conductor (strictly speaking, they should be called surface plasmon-polaritons to reflect this hybrid nature *(2)*). In this interaction, the free electrons respond collectively by oscillating in resonance with the light wave. The resonant interaction between the surface charge oscillation and the electromagnetic field of the light constitutes the SP and gives rise to its unique properties.

SPs help to concentrate light in subwavelength structures by using the different (relative) permittivities, ε, of the metals and the surrounding nonconducting media (ε is the square of the complex index of refraction). In this manner, concentrating light promotes an electric field enhancement that can be used to manipulate light-matter interactions and boost nonlinear phenomena. For example, metallic structures that are much smaller than the wavelength of light are vital to the massive signal enhancement achieved in surface-enhanced Raman spectroscopy (SERS)—a technique that can now detect a single molecule *(3, 4)*. Furthermore, the enhanced field associated with SPs makes them suitable for use as sensors, and commercial systems have already been developed for sensing biomolecules.

Surface plasmon resonance (SPR) biosensors are optical sensors that use special electromagnetic waves—surface plasmon-polaritons—to probe interactions between an analyte in solution and a biomolecular recognition element immobilized on the SPR sensor surface. Major application areas include the detection of biological analytes and analysis of biomolecular interactions, where SPR biosensors provide benefits for label-free real-time analytical technology.

An affinity biosensor consists of a transducer (electrochemical *(5)*, piezoelectric *(6)*, or optical *(7)*) and a biological recognition element that interacts with a selected analyte. Various optical methods have been exploited in biosensors including fluorescence spectroscopy *(8)*, interferometry (reflectometric white light interferometry *(9)* and modal interferometry in optical waveguide structures *(10)*, spectroscopy of guided modes of optical waveguides (grating coupler *(11)* and resonant mirror *(12)*, and surface plasmon resonance (SPR) *(13, 14)*. Fluorescence-based biosensors offer high sensitivity but, because of the use of labels, they require either multistep detection protocols or delicately balanced affinities of interacting biomolecules for displacement assays, causing sensor cross-sensitivity to nontarget analytes *(15)*. Sensors such as optical interferometers, grating couplers, resonant mirrors, and SPR rely on the measurement of binding-induced refractive index changes, and thus, are label-free technologies.

This application arises from the unique nanoparticle optical properties of certain materials, such as silver and gold *(16)*.

It is now well established that optical excitation of the localized surface plasmon resonance (LSPR) of silver and gold nanoparticles results in absorption with extremely large molar extinction coefficients of ~3×10^{11} M^{-1} cm^{-1} *(17, 18)*, resonant Rayleigh scattering *(19, 20)* with an efficiency equivalent to that of 10^6 fluorophores *(21, 22)*, and strong enhancement of the local electromagnetic fields near the nanoparticle surface *(23, 24)*. Furthermore, the peak extinction or resonant Rayleigh scattering wavelength, λ_{max}, intensity, and line width of these LSPR spectra are strongly dependent on their size, shape, interparticle spacing, and local dielectric environment *(17, 24–28)*. Consequently, five different nanoparticle-based sensing mechanisms that enable the transduction of macromolecular or chemical binding events into optical signals have been introduced. These mechanisms are:

1. Resonant Rayleigh scattering from nanoparticle labels in a manner analogous to fluorescent dye labels *(16, 19, 21, 22)*.
2. Nanoparticle aggregation *(29, 30)*.
3. Charge-transfer interactions at nanoparticle surfaces *(25, 31, 32)*.
4. Local refractive index changes *(32–35)*.
5. Surface-enhanced Raman scattering *(36)*.

The optical-field enhancement from plasmon resonance at spheroids is studied by solving Maxwell's equations using spheroidal vector wave functions *(37)*. This treatment is an extension of the Mie theory for spheres. The optical-field enhancement at the end of a sharp tip has been used in surface-enhanced Raman spectroscopy (SERS). The optical-field enhancement will increase the Raman signals such that spectra of single molecules are possible. Single-molecule SERS experiments on Ag and Au colloids have indicated signal-to-noise enhancement factors of 10 to 15 orders of magnitude. Because the spectroscopic signal-to-noise enhancement goes as the fourth power of the field enhancement (light power two ways), the field enhancement would then be approximately three orders of magnitude at the detection spots. Theoretical studies of the optical-field enhancement at prolate spheroids show strong enhancements in the quasistatic limit. The field enhancement factor at the end of a spheroid is calculated by the finite-element time-domain (FETD) method. The enhancement factor strongly depends on the ratio of the wavelength to the structure size. The enhancement falls off rapidly as the structure size is enlarged; this is confirmed by our calculations. This is attributed to phase retardation or dephasing effects. The exactly solvable model of a spheroid shows that there are plasmon resonance regions with strong-field enhancements in the nonstatic regime and shows how their positions in parameter space and their magnitudes are related. In fact, there is a strong dependence on the parameters' wavelength, spheroidal length,

axial ratio, polarization, angle of incidence, and material properties. These sometimes very sensitive spots in the space spanned by these parameters may be used for specific sensing of the near environment of the spheroids.

It was also suggested in **ref.** *(37)* that the strong enhanced optical field caused by surface plasmon resonance could be used for trapping single fluorescent molecules. Because both attractive as well as negative forces are possible depending on the wavelength of the optical field, a molecule could be taken into the trap and then, by changing the optical wavelength, taken out of the trap. At the same time, the molecule could be investigated through SERS.

2. Fundamentals of Surface Plasmon Resonance

2.1. Coupling to Surface Plasmons

The interaction between the surface charges and the electromagnetic field that constitutes SP has two consequences (*see* **Fig. 1**). First, the interaction between the surface charge density and the electromagnetic field results in the momentum of the SP mode, $\hbar k_{SP}$, which is greater than that of a free-space photon of the same frequency, $\hbar k_0$ ($k_0 = \omega/c$ is the free-space wave vector). The charge density wave is associated with an electromagnetic wave; the field vectors of which reach their maxima at the interface and decay evanescently into both media. This surface plasma wave (SPW) is a transverse-magnetic (TM) polarized wave (the magnetic vector is perpendicular to the direction of propagation of the SPW and parallel to the plane of interface) and is characterized by the propagation constant and electromagnetic field distribution. Solving Maxwell's equations under the appropriate boundary conditions yields the SP dispersion relation *(38)*, that is, the frequency-dependent SP wave vector, k_{SP},

$$k_{SP} = k_0 \sqrt{\frac{\varepsilon_d \varepsilon_m}{\varepsilon_d + \varepsilon_m}}. \qquad (1)$$

The frequency-dependent permittivity of the metal, ε_m, and the dielectric material, ε_d, must have opposite signs if SPs are possible at such an interface. This condition is satisfied for metals (gold and silver are the most commonly used) because ε_m is both negative and complex (the latter corresponding to absorption in the metal). The real and imaginary parts of the propagation constant describe spatial periodicity and attenuation of an SPW in the direction of propagation, respectively *(39)*. As an example, using **Eq.1**, the SP wave vector for a silver-air interface in the red part of the visible spectrum is found to be $k_{SP} \cong 1.03 k_0$. This increase in

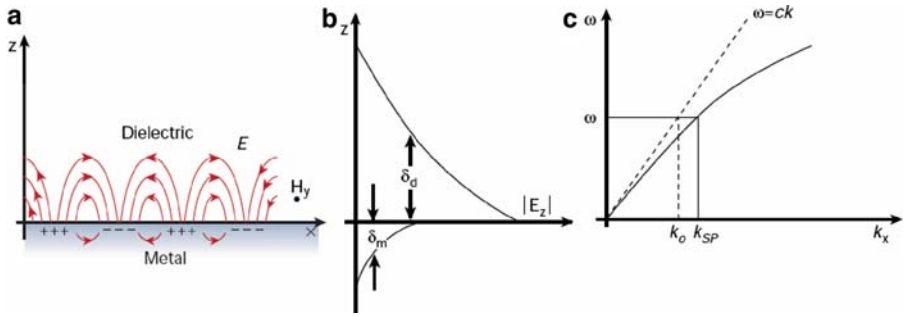

Fig. 1. SPs at the interface between a metal and a dielectric material have a combined electromagnetic wave and surface charge character, as shown in (**a**). They are transverse magnetic in character (H is in the *y* direction), and the generation of surface charge requires an electric field normal to the surface. This combined character also leads to the field component perpendicular to the surface being enhanced near the surface and decaying exponentially with distance away from it. (**b**) The field in this perpendicular direction is said to be evanescent, reflecting the bound, nonradiative nature of SPs, and prevents power from propagating away from the surface. In the dielectric medium above the metal, typically air or glass, the decay length of the field, δ_d, is on the order of half the wavelength of light involved, whereas the decay length into the metal, δ_m, is determined by the skin depth. (**c**) The dispersion curve for a SP mode shows the momentum mismatch problem that must be overcome to couple light and SP modes together with the SP mode lying beyond the light line, that is, it has greater momentum $\hbar k_{SP}$ than a free space photon $\hbar k_{SP}$ of similar frequency ω ***(40)***. Reproduced from **ref.*(40)*** with permission from Nature Publishing Group.

momentum is associated with SP binding to the surface and the resulting momentum mismatch between light and SPs of similar frequency must be bridged if light is used to generate SPs.

The second consequence of the interaction between the surface charges and the electromagnetic field is that, in contrast to the propagating nature of SPs along the surface, the field perpendicular to the surface decays exponentially with distance from the surface. The field in this perpendicular direction is said to be evanescent or near field in nature and is a consequence of the bound, nonradiative nature of SPs, which prevents power from propagating away from the surface.

There are three main techniques by which the missing momentum can be provided. The first makes use of prism coupling to enhance the momentum of the incident light ***(41, 42)***. The second involves scattering from a topological defect on the surface, such as a subwavelength protrusion or hole, which provides a convenient way to generate SPs locally ***(43, 44)***. The third makes use of a periodic corrugation on the metal's surface ***(45)***.

2.2. Surface Plasmon Propagation

Once light has been converted into an SP mode on a flat metal surface, it will propagate but will gradually attenuate because of losses arising from absorption in the metal. This attenuation depends on the dielectric function of the metal at an oscillation frequency of SP. The propagation length, δ_{SP}, can be found by seeking the imaginary part, k''_{SP}, of the complex surface plasmon wave vector, $k_{SP} = k'_{SP} + ik''_{SP}$, from the SP dispersion **Eq.1** ***(46)***,

$$\delta_{SP} = \frac{1}{2k''_{SP}} = \frac{c}{\omega}\left(\frac{\varepsilon'_m + \varepsilon_d}{\varepsilon'_m \varepsilon_d}\right)^{\frac{3}{2}} \frac{(\varepsilon'_m)^2}{\varepsilon''_m}, \quad (2)$$

where ε'_m and ε''_m are the real and imaginary parts of the dielectric function of the metal, $\varepsilon_m = \varepsilon'_m + i\varepsilon''_m$. Silver is the metal with the lowest losses in the visible spectrum: propagation distances are typically in the range of 10–100 μm, increasing toward 1 mm as one moves into the 1.5-μm near-infrared telecom band (*see* **Fig. 2**). In the past, absorption by the metal was considered a significant problem because SPs were not thought to be viable for photonic elements; the SP propagation length was smaller than the size of components at that time. This view is now changing thanks to recent demonstrations of SP-based components that are significantly smaller than the propagation length *(47)*. Such developments pave the way for the integration of many SP-based devices into circuits before propagation losses become too significant. In addition to dealing with the problem of loss owing to absorption in the metal, another key loss mechanism must be considered, that is, unwanted coupling to radiation. To build SP-based circuits one will need components that convert one SP mode into another, for example, a switch to reroute SPs without

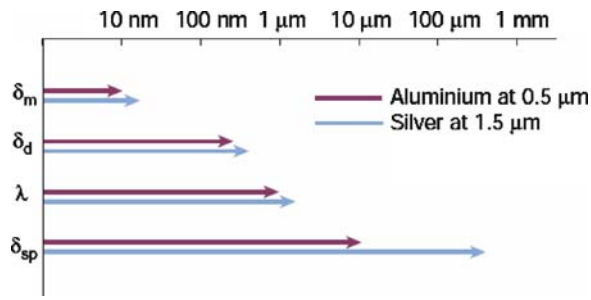

Fig. 2. Three characteristic length scales are important for SP-based photonics in addition to that of the associated light. The propagation length of the SP mode, δ_{SP}, is usually dictated by loss in the metal. For a relatively absorbing metal such as aluminum, the propagation length is 2 μm at a wavelength of 500 nm. For a low-loss metal, for example, silver, at the same wavelength, the propagation length is increased to 20 μm. By moving to a slightly longer wavelength, such as 1.55 μm, the propagation length is further increased toward 1 mm. The propagation length sets the upper size limit for any photonic circuit based on SPs. The decay length in the dielectric material, δ_d, is typically on the order of half the wavelength of light involved and dictates the maximum height of any individual features and components that might be used to control SPs. The ratio of δ_{SP} thus provides a measure of the number of SP-based components that may be integrated together. The decay length in the metal, δ_m, determines the minimum feature size that can be used; as shown in the diagram, this is between one and two orders of magnitude smaller than the wavelength involved, thus highlighting the need for good control of fabrication on the nanometer scale. These combinations provide an indication of range for poor (Al at 0.5 μm) to good (Ag at 1.5 μm) SP performance *(40)*. Reproduced from **ref.*(40)*** with permission from Nature Publishing Group.

scattering the SP mode in a manner that results in the lose of energy to freely propagating light.

2.3. Surface Plasmon Band Structure and Periodic Surfaces

One of the key developments in photonics in the past 15 years has been photonic bandgap (PBG) materials. These synthetic materials use wavelength-scale periodic structures to manipulate the interaction between light and matter to build new photonic structures, such as photonic crystal fiber *(48)*. These developments have been predominantly made in periodically structured insulating and semiconducting materials. By making use of SPs, metals can also be used as PBG materials in the form of photonic surfaces *(49)*.

The nature of SPs changes when they propagate on metal surfaces that are periodically textured on the scale of the wavelength of light. When the period of the nanostructure is half that of the effective wavelength of the SP mode, scattering may lead to the formation of SP standing waves and the opening of an SP stop band *(49) see* **Fig. 3**). When the surface is modulated in both in-plane directions, for example by a periodic array of bumps, SP modes may be prevented from traveling in any in-plane direction, thus leading to a full PBG for SP modes *(49, 51)* (*see* **Fig. 4**). **Figure 4** provides a nice demonstration of how the problems associated with absorption by the metal can be overcome. It demonstrates that, although finite, the SP propagation length is more than enough to enable the SP to experience many periods of the textured surface, and thus, display the PBG phenomenon.

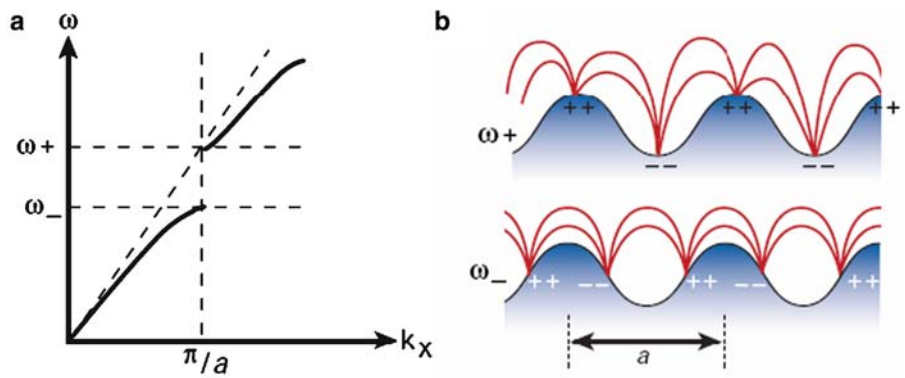

Fig. 3. Periodic texturing of the metal surface can lead to the formation of an SP photonic bandgap when the period, *a*, is equal to half the wavelength of the SP, as shown in the dispersion diagram (**a**). Similar to electron waves in crystalline solids, there are two SP standing wave solutions, each with the same wavelength but, owing to their different field and surface charge distributions, they are of different frequencies. The upper frequency solution, *v*&, is of higher energy because of the greater distance between the surface charges and the greater distortion of the field, as shown schematically in (**b**). SP modes with frequencies between the two band edges, *v*& and *v*–, cannot propagate, and, as a result, this frequency interval is known as a stop gap. By providing periodic texture in two dimensions, SP propagation in all in-plane directions can be blocked, leading to the full bandgap for SPs. At the band edges, the density of SP states is high, and there is a significant increase in the associated field enhancement ***(40)***. Reproduced from **ref.*(40)*** with permission from Nature Publishing Group.

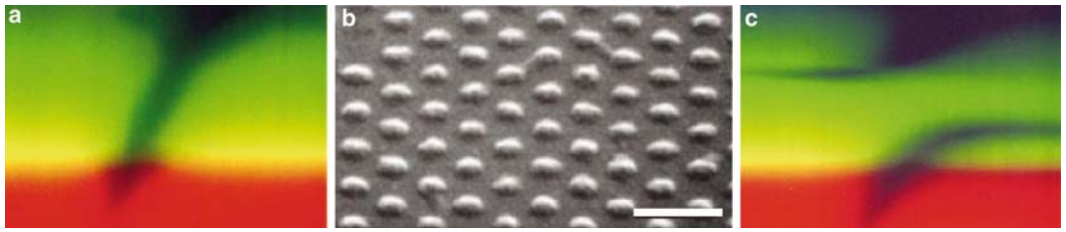

Fig. 4. SP photonic bandgap. The SP dispersion curve shown in **Fig. 1** was directly imaged using a modified prism coupling technique. (**a)** The dispersion curve (here shown as inverse wavelength versus angle) for a flat surface is shown in the upper picture; here, dark regions correspond to the coupling of incident light to the SP mode, and the colors are produced on a photographic film by the wavelength of the light used. (**b**) If the metal surface is textured with a two-dimensional pattern of bumps on an appropriate length scale (roughly half the wavelength of light) as shown in this scanning electron microscopy (SEM) image, a bandgap is introduced into the dispersion curve of the associated SP modes. Bar, 0.7 mm. (**c**) The bandgap is clearly seen in the lower pictures, where there is a spectral region in which no SP mode (as indicated by the dark regions) exists. Also, note the distortion of the SP mode and the edges of the bandgap ***(40)***. Reproduced from **ref.*(40)*** with permission from Nature Publishing Group.

We also note with interest that recent developments in the fabrication of periodic nanostructures via self-assembly offer the prospect of easily producing SP PBG substrates to act as photonic substrates on which to define SP photonic circuits.

At frequencies within a band gap, the density of SP modes is zero—no SP modes can be supported. However, at the band edges, the SP mode dispersion is flat and the associated density of SP modes is high, corresponding to a high field enhancement close to the metal surface. Additionally, the nature of this flat band signifies that such modes can be excited by incident light over a wide range of angles, making them good candidates for frequency-selective surfaces. Flat bands are also associated with the localized SP modes of metallic nanoparticles *(52)*. The frequency and width of these modes are determined by the particle's shape, material, size and environment *(52–54)*, and, for this reason, they are being pursued as tags for biosensing *(54, 55)*, and as substrates for SERS *(57)*, and potentially as aerials for fluorophores *(57, 58)*. The interaction between two or more nanoparticles can lead to additional levels of field enhancement *(60–62)*, with even more dramatic effects associated with hot spots in random structures *(63)*.

3. Materials

1. Gold substrates for SPR experiments were prepared using vapor deposition to deposit 48-nm-thick Au films onto 18 × 18-mm × 0.45-mm-thick SF-10 glass (η = 1.727) cover slips (Schott Glass Technologies, Durea, PA).

2. Water used in making solutions and for washing the samples was reverse-osmosis purified (18 MΩ cm).
3. A standard hybridization buffer and contains 0.3 M NaCl, 20 mM sodium phosphate, 2 mM EDTA, adjusted to pH 7.4 with NaOH (2-SSPE), plus 0.2% (w/v) (6.9 mM) sodium dodecyl sulfate (SDS).
4. 11-Mercaptoundecanoic acid (MUA) was from Aldrich (Milwaukee, WI), poly(L-lysine) (PL) was from Sigma (St. Louis, MO), and 1,4-phenylenediisothiocyanate (PDITC) was from Aldrich.
5. MUA monolayers were prepared on clean vapor-deposited gold substrates, and a layer of PL was electrostatically adsorbed onto the MUA surface (*see* **Note 1**).
6. Pyridine.
7. Dimethylformamide (DMF).
8. 0.1 M sodium bicarbonate buffer, pH 9.0, containing 0.5 M NaCl.
9. NH_4OH.
10. A Kretschmann-configuration imaging SPR instrument.
11. Resistive thermofoil heating elements (Minco Products Inc., Minneapolis, MN) attached to the cell, with miniature platinum RTD sensors (Minco) embedded in the cell for feedback temperature control with a Love 1600 series self-tuning PID temperature controller (Love Controls, Wheeling, IL).
12. Molecular Dynamics FluorImager 575 (Sunnyvale, CA).

4. The Principle Underlying Surface Plasmon Resonance Detection

Because the vast majority of the field of an SPW is concentrated in the dielectric, the propagation constant of the SPW is extremely sensitive to changes in the refractive index of the dielectric. This property of SPW underlies the physical principle of affinity SPR biosensors—biomolecular recognition elements on the surface of metal recognize and capture analytes present in a liquid sample producing a local increase in the refractive index at the metal surface. The refractive index increase promotes an increase in the propagation constant of SPW propagating along the metal surface (*see* **Fig. 5**), which can be accurately measured by optical means.

The magnitude of the change in the propagation constant of an SPW depends on the refractive index change and its distribution with respect to the profile of the SPW field. There are two limiting cases:

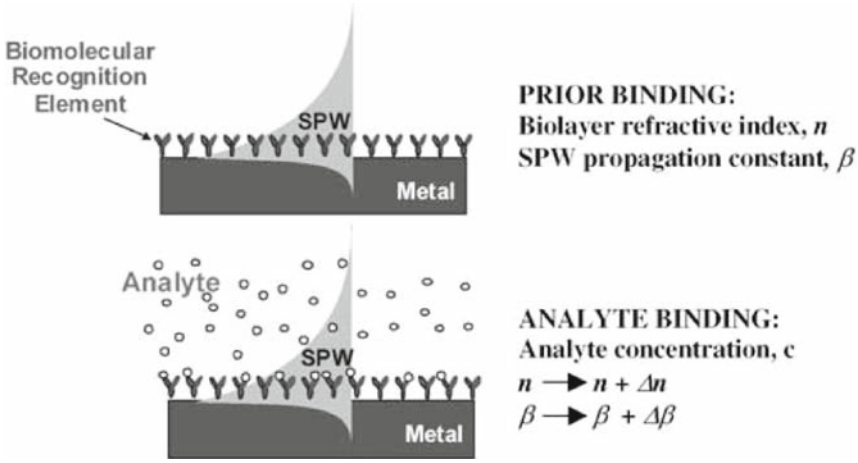

Fig. 5. Principle of SPR biosensing *(64)*. Reproduced from **ref.***(64)* with permission from Springer.

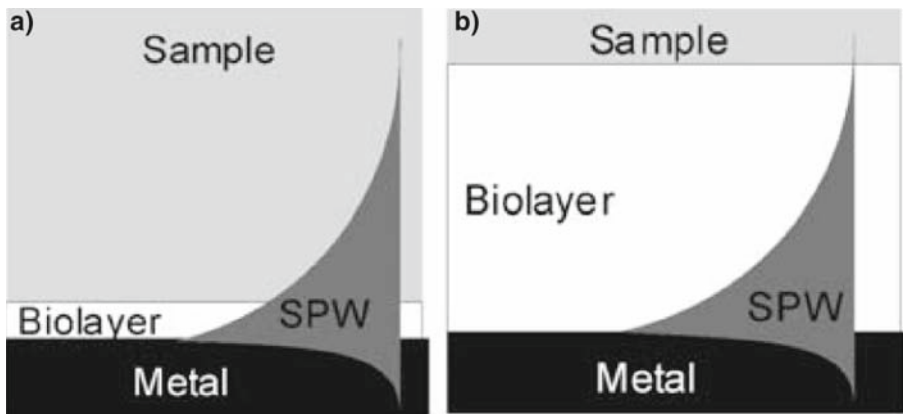

Fig. 6. Surface plasmon-polariton probing: (**a**) biomolecular interactions occurring within a short distance from the metal surface, and (**b**) biomolecular interactions occurring within the entire extent of the SPW field *(64)*. Reproduced from **ref.** *(64)* with permission from Springer.

1. Analyte capture occurs only within a short distance from the metal surface **(Fig. 6a)**.
2. Analyte capture occurs within the whole extent of the SPW field **(Fig. 6b)**.

Perturbation theory *(65)* suggests that if the binding occurs within the entire depth of the SPW field (**Fig. 6b**), the binding-induced refractive index change, Δn, produces a change in the

real part of the propagation constant, $\Delta\beta$, which is directly proportional to the refractive index change:

$$\mathrm{Re}\{\Delta\beta\} \cong k\Delta n\,, \tag{3}$$

where k denotes the free-space wave number ***(66)***. If the refractive index change is caused by a binding event occurring within a distance from the surface d that is significantly smaller than the penetration depth of the SPW, the corresponding change in the real part of the propagation constant can be expressed as follows:

$$\mathrm{Re}\{\Delta\beta\} \cong \frac{2n_s n_f k^2 d}{\sqrt{|\mathrm{Re}\{\varepsilon_m\}|}}\Delta n = Fk\Delta n\,, \tag{4}$$

where n_f and n_s denote the refractive index of the biolayer and the refractive index of the background dielectric medium (sample), respectively. The binding-induced change in the propagation constant of SPW is proportional to the refractive index change and the depth of the area within which the change occurs. The factor F ($F < 1$) accounts for the fact that the interaction occurring within a thin layer is probed only by a fraction of the SPW field.

5. Concept of Surface Plasmon Resonance Optical Chemical Sensors and Biosensors (Excitation and Interrogation of Surface Plasmon-Polaritons)

In SPR sensors, an SPW is excited by a light wave and the effect of this interaction on the characteristics of the light wave is measured. From these measurements, changes in the propagation constant of the SPW can be determined. SPW excitation by light can occur only if the component of the light's wave vector parallel to the metal surface matches that of the SPW. This can be achieved by means of prism coupling, waveguide coupling, and grating coupling.

Generally, an SPR optical sensor comprises an optical system; a transducing medium, which interrelates the optical and (bio) chemical domains; and an electronic system supporting the optoelectronic components of the sensor and allowing data processing. The transducing medium transforms changes in the quantity of interest into changes in the refractive index, which may be determined by optically interrogating the SPR. The optical part of the SPR sensor contains a source of optical radiation and an optical structure in which SPW is excited and interrogated. In the process of interrogating the SPR, an electronic signal is generated and

processed by the electronic system. Major properties of an SPR sensor are determined by properties of the sensor's subsystems. The sensor sensitivity, stability, and resolution depend on properties of both the optical system and the transducing medium. The selectivity and response time of the sensor are primarily determined by the properties of the transducing medium.

The interaction of a light wave with an SPW can alter the light's characteristics, such as amplitude, phase, polarization, and spectral distribution. Changes in these characteristics can be correlated with changes in the propagation constant of the SPW. Therefore, binding-induced changes on the refractive index at the sensor surface and, consequently, the propagation constant of the SPW can be determined by measuring changes in one of these characteristics. Based on the measured characteristic, SPR biosensors can be classified as angle, wavelength, intensity, phase, or polarization modulation-based sensors. In SPR sensors with angular modulation, the component of the light wave's wave vector parallel to the metal surface matching that of the SPW is determined by measuring the coupling strength at a fixed wavelength and multiple angles of light wave incidence and determining the angle of incidence yielding the strongest coupling (**Fig. 7a**, upper plot). In SPR sensors with wavelength modulation, the component of the light wave's wave vector parallel to the metal surface matching that of SPW is determined by measuring the coupling strength at a fixed angle of incidence and multiple wavelengths and determining the wavelength yielding the strongest coupling **(Fig. 7b)**. In SPR sensors with intensity modulation, the change in the intensity of the light wave interacting with SPW is measured at a fixed wavelength and angle of incidence **(Fig. 7b)**. In SPR sensors with phase modulation, a shift in the phase of the light wave interacting with the SPW is measured at a fixed wavelength and angle of incidence (**Fig. 7a**, lower plot). In SPR sensors with polarization modulation, changes in the polarization are measured at a fixed wavelength and angle of incidence.

6. Methods

6.1. Surface Plasmon Resonance Sensors Using Attenuated Total Reflection Optical Prism Couplers

In configurations based on prism coupling, a light wave passes through a high-refractive index prism and is totally reflected at the interface between a prism coupler and a thin metal layer (of the thickness of ~50 nm) and excites an SPW at the outer boundary of the metal by evanescently tunneling through the thin metal layer **(Fig. 8a)**. This evanescent wave propagates along the interface with a propagation constant, which can be adjusted to match that of SPW by controlling the angle of incidence. This method is

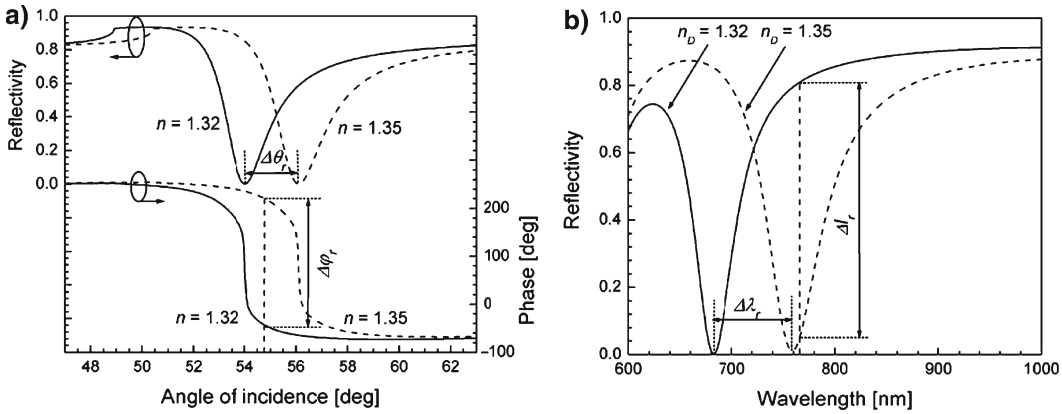

Fig. 7. Reflectivity and phase for a light wave exciting an SPW in the Kretschmann geometry (SF14 glass prism—50-nm-thick gold layer—dielectric) versus (**a**) the angle of incidence for two different refractive indices of the dielectric (wavelength 682 nm), and (**b**) wavelength for two different refractive indices of the dielectric (angle of incidence 54°) ***(64)***. Reproduced from **ref.*(64)*** with permission from Springer.

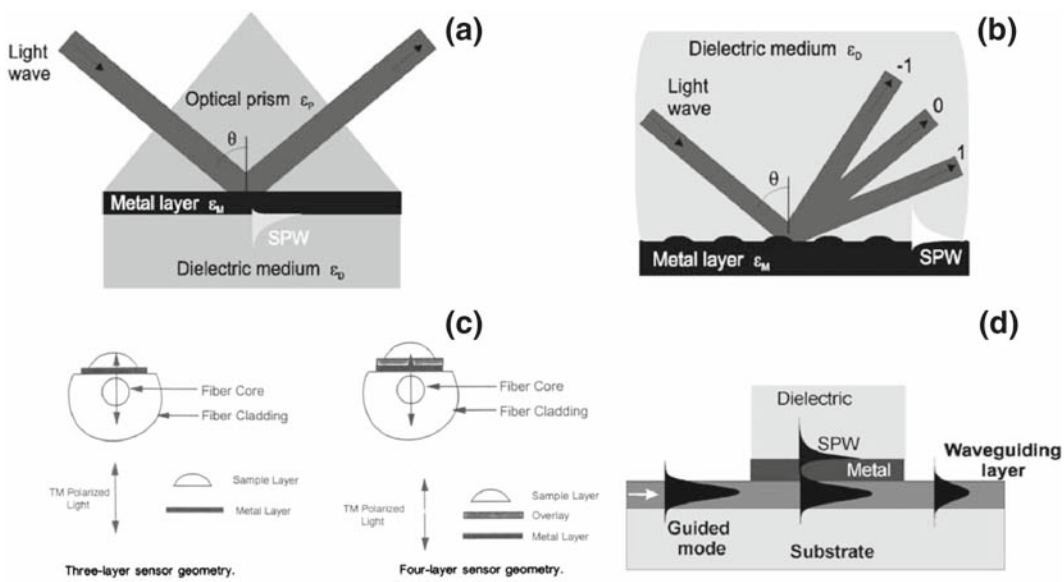

Fig. 8. Excitation of surface plasmon-polaritons: (**a**) by a light beam via prism coupling; (**b**) by light diffraction on a diffraction grating; (**c**) by optical fibers of a waveguide; and (**d**) by a guided mode of an optical waveguide ***(64,99)***. Reproduced from **ref.*(64)*** with permission from Springer and from **ref.*(99)*** with permission from American Chemical Society.

referred to as the attenuated total reflection (ATR) method *(67)*. Particularly, the Kretschmann geometry of the ATR method has been found to be suitable for sensing and has become the most widely used geometry in SPR sensors. In this configuration, a light wave is totally reflected at the interface between a prism coupler and a thin metal layer (of the thickness of ~50 nm) and excites an SPW at the outer boundary of the metal by evanescently tunneling through the thin metal layer. All of the main detection approaches have been demonstrated in SPR prism-based sensors, such as measurement of the intensity of the reflected light wave *(68, 69)*, measurement of the resonant angle of incidence of the light wave *(70, 71)*, and measurement of the resonant wavelength of the incident light wave *(72)*. Prism-based SPR sensors using angular interrogation have been extensively studied at Linköping University (Sweden) *(71)* and by Biacore (Sweden) *(73, 74)*.

The sample (*see* **Note 2**) was illuminated with p-polarized, collimated light from a 632.8-nm, 1.5-mW HeNe laser (Uniphase Model 1101P, Manteca, CA), coupled through a MgF_2 antireflection-coated SF-10 (η = 1.727) 30 × 30 × 30-mm equilateral glass prism (Ealing Electro-Optics, Holliston, MA) and η = 1.725 index-matching fluid (Cargille, Cedar Grove, NJ) to the sample. The reflected light from the surface was imaged onto a CCD camera (either a Panasonic Model WV-BL200 [Panasonic Broadcast & Television Systems Co., Secaucus, NJ] or an iSight iSC2050 [iSight, Inc., Cedar Knolls, NJ] was used, depending on when the experiment was performed), and the image was digitized by a frame grabber (Video Blaster RT300 [Creative Labs, Inc., Milpitas, CA] or Data Translation DT3155 [Data Translation, Marlboro, MA]) and AdobeCap Video Capture Utility v1.1 (Adobe Systems, San Jose, CA) or Data Translation Acquire To Host Application v1.0 software running on a Dell computer platform (*see* **Note 3**).

In traditional multichannel SPR sensors, SPWs were excited via a prism coupler in multiple areas that were arranged perpendicularly to the direction of propagation of SPWs; the angular or spectral distribution of reflected light was analyzed to yield information about the measurement in each channel. Although this spectroscopic approach led to the development of high-performance SPR sensing devices, the number of sensing channels that could be realized using this approach was rather limited (<10). To increase the number of sensing channels, various SPR sensor approaches have been proposed. One approach is based on SPR imaging in which a collimated light beam from a polychromatic light source passes through a prism and is made incident on an SPR-active metal layer; the reflected light is detected with a CCD camera after passing through a narrowband interference filter. This approach has been demonstrated for monitoring adsorption

of a single-stranded DNA-binding protein onto single-stranded DNA patterned into an array of 500 × 500-μm squares (*see* **Note 4**). The operating wavelengths for imaging SPR sensors have been selected for different applications. An alternative approach is based on detection of spatial changes in the phase of light exciting an SPW and interferometry. Two interferometric schemes have been proposed. In the Mach-Zehnder interferometer-based scheme, monochromatic light was split into reference and signal beams; the signal beam passed through a prism and, after reflection from an SPR-active metal layer, was recombined with the reference beam, producing an interference pattern on a CCD camera. In the transverse electric (TE)–TM polarization interferometer, TE and TM polarized beams passed through a prism and, after reflection from an SPR-active surface, were shifted with respect to each other and recombined by means of a polarizer producing an interference pattern on a CCD camera. Another interesting approach is based on SPR microscopy and uses surface scanning and SPWs excited by means of an objective lens. Most recently, a new approach has been proposed that is based on spectroscopy of SPW on an array of diffraction gratings.

6.2. Surface Plasmon Resonance Sensors Using Grating Couplers

An SPW can be excited by diffraction on a grating, **Fig. 8b**. The component of the wave vector of the diffracted waves parallel to the interface is diffraction increased by an amount that is inversely proportional to the grating period and can be matched to that of an SPW *(75)*. If a metal–dielectric interface is periodically distorted, the incident optical wave is diffracted, forming a series of beams directed away from the surface at a variety of angles *(76)*. The component of momentum of these diffracted beams along the interface differs from that of the incident wave by multiples of the grating wave vector. If the total component of momentum along the interface of a diffracted order is equal to that of the SPW, the optical wave may couple the SPW *(77)*. The mathematics involved in modeling the grating SPR-sensing structures is more complex than that of planar prism-based systems *(78, 79)*; therefore, modeling the response of grating-based SPR structures and analysis of sensor data is more difficult. Grating-based optical SPR sensors that use the measurement of SPR light intensity variations *(80, 81)* and the wavelength interrogation *(82, 83)* have been demonstrated. Although the interrogation optical systems for SPR sensors using prisms and grating couplers are essentially the same, accurate control of the thickness of the plasmon active metal layer is not required in the grating-based SPR sensors. A drawback for certain applications is that in grating-based SPR systems, unlike prism-based systems, the light beam is incident through the sample solution, and, therefore, the analyte and flow-cell need to be optically transparent.

6.3. Surface Plasmon Resonance Sensors Using Optical Waveguides

The use of optical waveguides in SPR sensors provides numerous attractive features such as a simple method of controlling the optical path in the sensor system (efficient control of properties of the light, suppression of the effect of stray light, etc.), small size, and ruggedness. The process of exciting an SPW in optical waveguide-based SPR-sensing structures is, in principle, similar to that in the ATR coupler. A light wave is guided by the waveguide and, entering the region with a thin metal overlayer, it evanescently penetrates through the metal layer. If the SPW and the guided mode are phase matched, the light wave excites an SPW at the outer interface of the metal. Theoretically, the sensitivity of waveguide-based SPR devices is approximately the same as that of the corresponding ATR configurations. Despite increased design constraints compared with bulk prism-based SPR-sensing devices, all of the main SPR detection approaches have been implemented in waveguide SPR sensors.

6.3.1. Surface Plasmon Resonance Sensors Based on Optical Fibers

Currently, optical fiber SPR probes present the highest level of miniaturization of SPR devices, allowing for chemical and biological sensing in inaccessible locations where the mechanical flexibility and the ability to transmit optical signals over a long distance make the use of optical fibers very attractive (*see* **Fig. 8c**). The use of optical fibers for SPR sensing was first proposed by Jorgenson and Yee *(84)*. They used the wavelength interrogation technique and formed an SPR-sensing structure by using a conventional polymer-clad silica fiber with partly removed cladding and an SPR active metal layer deposited symmetrically around the exposed section of the fiber core. This approach allows construction of miniaturized optical fiber SPR probes with a limited interaction area at a length of approximately 10 mm. It has been demonstrated that the operating range of the sensor may be customized for sensor applications in the refractive index range 1–1.7 using a thin high-refractive index dielectric overlayer and high refractive index core fibers *(85)*. A similar structure, in which the SPR-sensing area is formed not at the tip but in the middle of an optical fiber, has been reported to be used as an intensity measurement-based sensor *(86, 87)*. In this configuration, a collimated monochromatic light beam is launched into a fiber in a fashion such that only modes with propagation constants within a narrow range are efficiently excited. Variations in the refractive index of the analyte are determined by measuring the transmitted optical power. The SPR sensor sensitivity is negatively influenced by exciting an SPW by fiber modes that are incident on the metal surface at slightly different angles. Generally, both types of multimode fiberoptic SPR-sensing devices may suffer from rather low stability. The modal distribution of light in the fiber is very sensitive to mechanical disturbance and disturbances occurring close to the sensing area of the fiber may cause intermodal coupling

and modal noise. Because of the cylindrical shape of the sensing area, fabrication of homogeneous SPR coatings and functionalization of the sensor's surface pose technological challenges. To overcome these drawbacks and allow for further reduction of the sensing area, SPR sensors based on single-mode optical fibers have been proposed *(88–90)*. A major drawback of optical fiber SPR sensors of this type is that they require reliable control of polarization state of the optical wave propagating in the fiber (e.g., by using polarization-maintaining optical fibers). Recently, an alternative configuration of a wavelength interrogation-based SPR sensor using a single-mode optical fiber was described *(91)*. In this configuration, SPW is excited on a metal-coated tapered single-mode optical fiber. It has been demonstrated that if the sensor is operated at wavelengths below 600 nm, it may be used for monitoring variations in the refractive index of aqueous media.

6.3.2. Surface Plasmon Resonance Sensors Based on Integrated Optical Waveguides

The process of exciting an SPW in an optical waveguide-based SPR structure **(Fig. 8d)** is similar to that in the ATR coupler. The light wave is guided by an optical waveguide and, when entering the region with a thin metal layer, it evanescently penetrates through the metal layer, exciting an SPW at its outer boundary. Integrated optical waveguide SPR sensors appear promising for the development of multichannel sensing devices on one chip with the potential for efficient referencing and multicomponent sensor analysis of complex samples. Various groups have developed SPR-sensing devices using slab *(92, 93)* and channel *(94, 95)* single-mode integrated optical waveguides. Similar to single-mode optical fiber SPR sensors, the integrated optical SPR-sensing devices exhibit a rather limited operating range. Various possibilities for tuning the operating range of the sensor have been explored, such as using waveguides fabricated on low refractive index glass *(94)*, a buffer layer *(93)*, a high refractive index overlayer *(96)*, and multilayer structures that are more complex *(97, 98)*. However, all of the approaches that introduced additional layers were found to yield less-sensitive SPR-sensing devices because of a relatively lower concentration of electromagnetic field in the analyte.

6.4. Imaging Fluorescence Detection

For detection of hybridization with fluorescently labeled targets, hybridization was performed by pipetting a small volume (20 μL) of hybridization solution onto the gold surface and "sandwiching" the droplet between the gold surface and a plain glass cover slip, which was laid on top. The sandwich assembly was enclosed in a petri dish on a platform above several milliliters of water, to provide a humid atmosphere to prevent drying of the sample during the hybridization period. After hybridization, the cover slip was removed and the gold surface washed by immersion in a beaker of 2-SSPE/0.2% SDS (*see* **Notes 4–6**). Finally, after washing, the sample was placed face down on top of the glass

scanner tray provided with a Molecular Dynamics FluorImager 575 (Sunnyvale, CA) with a droplet of 2-SSPE/0.2% SDS between the gold surface and the glass scanner tray to provide an aqueous environment during the scan. The sample was scanned in the FluorImager using the standard Scanner Control v.1.1 software provided with the instrument, using a 530 (15-nm) band-pass interference filter to select for the fluorescein label's fluorescence emission. The SPR images were imported into NIH Image v.1.61 software where they were filtered and cropped as necessary, and "Plot Profile" analysis was performed on selected regions. In a plot profile, the average pixel value for each column of pixels within a rectangular region is calculated and plotted against that column's position. Then, numerical values from each plot profile were exported as a text file, which was subsequently opened in Igor v.1.25 graphing software (WaveMetrics, Lake Oswego, OR), where plot profiles could be overlaid, offset, ratioed, etc. For analysis of fluorescence images, ImageQuaNT v.4.1 software (provided with the FluorImager) was used.

7. Performance Characteristics

The main performance characteristics relevant for SPR biosensors include sensitivity, accuracy, precision, repeatability, and the lowest detection limit. Sensor sensitivity, S, is the ratio of the change in sensor output, P (e.g., angle of incidence, wavelength, intensity, phase, and polarization of light wave interacting with an SPW), to the change in measurand (e.g., analyte concentration, c). SPR biosensor sensitivity can be broken down into two components—sensitivity to refractive index changes produced by binding of the analyte to biomolecular recognition elements on the sensor surface, S_{RI}, and the efficiency, E, with which the presence of analyte at a concentration c is converted into the change in the refractive index n:

$$S = \frac{\partial P}{\partial n}\frac{\partial n}{\partial c} = S_{RI}E\,. \tag{5}$$

The efficiency E depends on the properties of the biomolecular recognition elements and the target analyte. The refractive index sensitivity S_{RI} can be separated into two terms:

$$S_{RI} = \frac{\partial P}{\partial \mathrm{Re}\{\beta\}}\frac{\partial \mathrm{Re}\{\beta\}}{\partial n} = S_1 S_2. \tag{6}$$

The first term, S_1, depends on the modulation method and the method of SPW excitation ***(100–103)***. The S_2 term is independent

of the modulation method and the method of SPW excitation and describes the sensitivity of SPW's propagation constant to refractive index changes, **Eqs. 3** and **4**.

Accuracy describes the degree to which a sensor output represents the true value of the measurand (analyte concentration). Accuracy is often confused with *precision*, which refers to the manner in which repeated measurements conform without a reference to any true value. *Repeatability* refers to the capacity of a sensor to reproduce output reading under the same measurement conditions over a short interval of time. The *lowest detection limit* describes the lowest concentration of analyte that can be measured by the sensor.

8. SPR Biosensing Formats

An interaction between a biomolecular recognition element on an SPR sensor surface and an analyte in a liquid sample is governed by kinetic equations. To illustrate the fundamental properties of the interaction, we discuss the pseudo-first-order kinetic equation:

$$\frac{\mathrm{d}R}{\mathrm{d}t} = k_{\mathrm{a}} c\left(1 - R\right) - k_{\mathrm{d}} R\,, \tag{7}$$

where R is the relative amount of bound analyte, c is the analyte concentration, t is time, and k_{a} and k_{d} are the association and dissociation kinetic rate constants, respectively ***(104)***. This interaction model assumes a 1:1 binding, rapid mixing of the analyte from the bulk phase to the sensor surface layer, and single-step binding. Observed binding, however, may deviate from this simple model because of more complex mechanisms of interaction and mass transport limitations ***(105)***. **Equation 7** yields for R:

$$R(t) = \left[\frac{k_{\mathrm{a}} c}{k_{\mathrm{a}} c + k_{\mathrm{d}}} - R_0\right]\left(1 - e^{-\left(k_{\mathrm{a}} c + k_{\mathrm{d}}\right) t}\right) + R_0, \tag{8}$$

where R_0 denotes the initial amount of analyte bound at the time $t = 0$ ***(104)***.

Various measurement formats have been adopted in SPR biosensing to ensure that the monitored binding event produces a measurable sensor response. The most frequently used measurement formats are direct detection, sandwich assay, and inhibition assay. In the direct detection format, the analyte in a sample interacts with a biomolecular recognition element (antibody) immobilized on the sensor surface, **Fig. 9**. The resulting refractive index change is directly proportional to the concentration of the analyte.

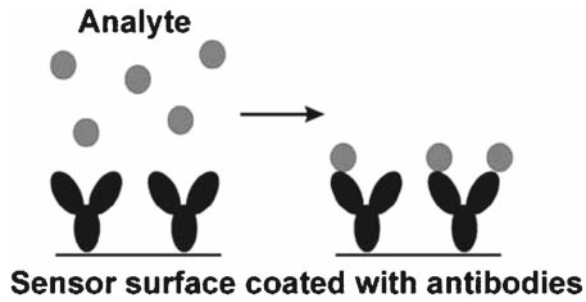

Fig. 9. Direct detection ***(64)***. Reproduced from **ref. *(64)*** with permission from Springer.

The kinetic model of the interaction between antibody and analyte suggests that the binding between the target analyte and the antibody is fast initially. As the interaction progresses, the binding rate gradually decreases and eventually reaches a state in which the association and dissociation processes are in equilibrium. The time required for the interaction to reach the equilibrium depends on the concentration of analyte and is longer for lower concentrations of analyte.

The dependence of the relative binding at equilibrium on the concentrations of analyte can be explained as follows: at low analyte concentrations, the equilibrium binding increases linearly with analyte concentration, whereas, at higher analyte concentrations, the binding sites provided by the biomolecular recognition elements are saturated and a further increase in the analyte concentration produces a smaller increase in the amount of bound analyte. The initial binding rate $\mathrm{d}R/\mathrm{d}t\,(t = 0)$ is directly proportional to the association rate constant and the analyte concentration. Both the amount of analyte bound at equilibrium and the initial binding rate can be used to determine analyte concentration. The measurement of the binding rate is faster and offers a larger dynamic range than the measurement of equilibrium binding. In the *sandwich assay format*, the measurement consists of two steps. In the first step, sample containing analyte is brought into contact with the sensor and the analyte molecules bind to the antibodies on the sensor surface. Next, the sensor surface is incubated with a solution containing secondary antibodies. The secondary antibodies bind to the previously captured analyte, further increasing the number of bound biomolecules **(Fig. 10)**, and, thus, the sensor response.

The *inhibition assay* is an example of a competitive assay. In this detection format, a sample is initially mixed with respective antibodies and then the mixture is brought into contact with the sensor surface coated with analyte molecules so that the unoccupied antibodies can bind the analyte molecules **(Fig. 11)**.

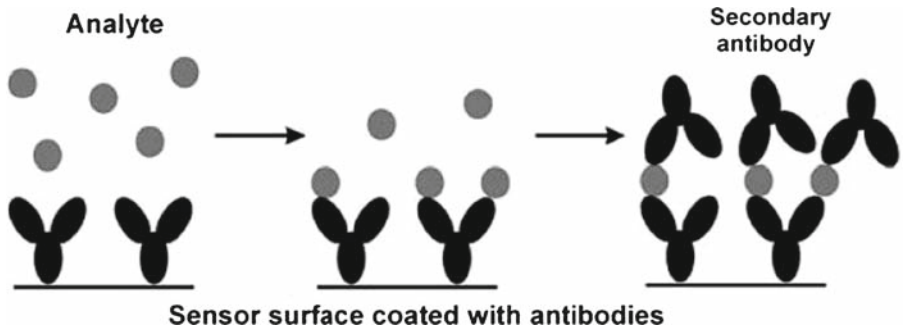

Fig. 10. Sandwich assay ***(64)***. Reproduced from **ref.** ***(64)*** with permission from Springer.

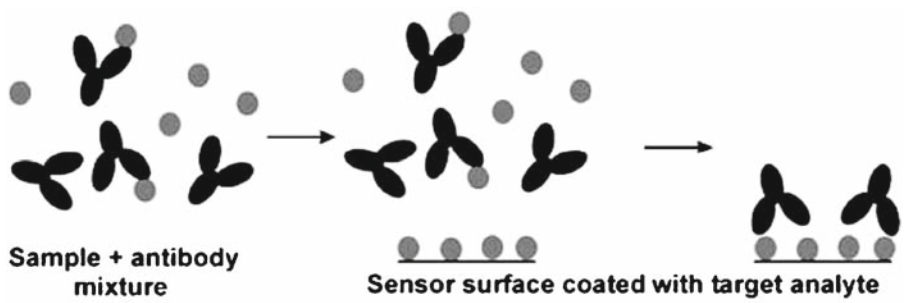

Fig. 11**.** Inhibition assay ***(64)***. Reproduced from **ref.** ***(64)*** with permission from Springer.

The amount of bound analyte over time may be estimated by calculating the equilibrium concentration of antibody that did not bind the analyte in the sample and then simulating the interaction between the unbound antibody and the analyte-derivatized surface.

9. Features and Challenges

SPR biosensor technology exhibits various advantageous features. In particular, these include:

1. Versatility—generic SPR sensor platforms can be tailored for the detection of any analyte, thereby providing a biomolecular recognition element that recognizes that the analyte is available; the analyte does not have to exhibit any special properties such as fluorescence or characteristic absorption and scattering bands.

2. No labels required—binding between the biomolecular recognition element and analyte can be observed directly without the use of radioactive or fluorescent labels.
3. Speed of analysis—the binding event can be observed in real time, providing a potentially rapid response.
4. Flexibility—SPR sensors can perform continuous monitoring as well as one-time analyses.

SPR biosensors exhibit two inherent limitations:

1. Specificity of detection—specificity is solely based on the ability of biomolecular recognition elements to recognize and capture analyte. Biomolecular recognition elements may exhibit cross-sensitivity to structurally similar but nontarget molecules. If the nontarget molecules are present in a sample at high concentrations, the sensor response caused by the nontarget analyte molecules may conceal specific responses produced by low levels of target analyte.
2. Sensitivity to interfering effects—similar to other affinity biosensors relying on the measurement of refractive index changes, SPR biosensor measurements can be compromised by interfering effects, which produce refractive index variations. These include nonspecific interactions between the sensor surface and sample (adsorption of nontarget molecules by the sensor surface) and background refractive index variations (caused by sample temperature and composition fluctuations).

10. Applications of SPR Biosensors

Two major application areas for SPR biosensing are the detection and identification of biological analytes and the biophysical analysis of biomolecular interactions. This review focuses on applications for detection and identification of biological analytes; recent advances in SPR-based biomolecular interaction analysis can be found in **ref.** ***(106)***.

Numerous SPR biosensors have been developed for the detection and identification of specific analytes. These biosensors use a number of platform designs, biomolecular recognition elements, and detection formats. The choice of detection format for a particular application depends on the size of the target analyte molecules, the binding characteristics of the biomolecular recognition elements, and the range of measured analyte concentrations. Direct detection is usually preferred in applications where direct binding of known concentrations of analyte produce a sufficient response. If necessary, the lowest detection limits of

the direct SPR biosensors can be improved by using a sandwich assay. The secondary antibodies may also be coupled to large particles such as latex particles *(107)* and gold beads *(108)* to further enhance the SPR sensor response. Smaller analytes (molecular weight <1,000) are usually measured using an inhibition assay.

11. Future Trends in Development of Surface Plasmon Resonance Sensors

Detection and analysis of chemical and biochemical substances are needed in many important areas, including medicine, environmental monitoring, biotechnology, and drug and food monitoring. Surface plasmon resonance sensor technology has potential for applications in these areas. Currently, SPR biosensor devices compete with other types of biosensors *(109)*, however, the major competitors of biosensors are immunoassays, which are commonly and widely used for the determination of numerous important substances and offer low-cost tests of high specificity and sensitivity. Today, commercially available biosensors cover a very limited area of the biochemical monitoring market, aiming primarily at research and analytical laboratories. To expand the market from specialized laboratories and centralized testing sites and gain a fair share of the biochemical monitoring market, SPR sensors have to compete with existing technologies on the basis of factors such as low cost, ease of use, robustness, sensitivity, and stability. It is envisaged that this will drive research and development of SPR-sensing devices in the following directions:

1. Improvement of detection limits. Current direct SPR biosensors are limited to the detection of approximately 1 pg mm^{-2} surface coverage of biomaterials, which is not sufficient for detecting low concentrations of low molecular weight analytes. Although further optimization of SPR optical instruments and development of efficient referencing concepts and sophisticated data-processing methods may improve the resolution of SPR-sensing devices and lower the detection limits, at present, no approach that can decrease this limit of detection by orders of magnitude is available.
2. Multichannel performance. Multichannel SPR sensors are required for direct detection in high-throughput screening systems in the search for new pharmaceuticals. The first steps in this direction include the system introduced by Biacore and the approach proposed by Berger *(109)*, which uses a 4-channel chip that can be rotated by 90° to provide 16 channels.
3. Development of advanced recognition elements. For applications of SPR sensors in complex realistic samples (e.g., blood),

advanced stable receptor matrices, which allow for resolving sensor responses from nonspecific background effects, will have to be developed.

Undoubtedly, in the future, SPR technology will benefit from the use of optical waveguide technology, which offers the potential for the development of miniaturized, compact, and rugged sensing elements with prospects of fabricating multiple sensors on one chip.

12. Notes

1. PDITC was then reacted with the surface by immersion for 2 h in a room temperature solution of 0.2% (w/v) PDITC in 10% pyridine/90% dimethylformamide (DMF), after which the sample was washed (first with DMF and then with ethanol) and then dried under a stream of nitrogen, leaving an isothiocyanate-derivatized surface.
2. Test droplets in 0.1 M sodium bicarbonate buffer, pH 9.0, containing 0.5 M NaCl were spotted onto the hydrophobic surface and left to react for 2 h at 37°C in a humid environment to prevent the spots from drying out. To stop the coupling reaction, the samples were immersed for 2 min in room temperature 1% NH_4OH, washed two times for 5 min each wash in room temperature H_2O, and finally blown dry under a stream of nitrogen, at which point they were ready to use for hybridization.
3. In all cases, the image data were recorded as an 8-bit grayscale image. The image acquisition systems were tested and shown to have a linear response to incident light intensity in the range used in the experiments.
4. For the DNA hybridization experiments, a special in situ cell was constructed, in which a Kel-F block (PCTFE, 3 M Industrial Chemical Products Division, St. Paul, MN) and a ½-in.-inner diameter Viton fluoroelastomer *O*-ring (Du Pont Dow Elastomers, L.L.C., Wilmington, DE) were sealed against the gold surface, to contain a small volume of liquid in contact with the central region of the gold surface. The cell was fitted with an inlet and outlet for replacing the cell contents by means of a syringe. The total system volume (inlet to outlet) was found to be 200 μL. The sample stage was rotatable through a large angular distance to find the optimal observation angle for a given sample but was locked at a fixed angle for the course of a hybridization experiment.

5. The cell could be flushed with 2-SSPE/0.2% SDS buffer to remove any unhybridized target DNA if desired.
6. To begin hybridization, a total volume of at least 300 μL of hybridization solution was injected into the in situ SPR cell using a syringe. Hybridization proceeded at room temperature while the SPR image was continuously monitored. After hybridization, in experiments where it was necessary to remove mismatched hybrids, the cell temperature was gradually raised using resistive thermofoil heating elements attached to the cell, with miniature platinum RTD sensors (Minco) embedded in the cell for feedback temperature control with a Love 1600 series self-tuning PID temperature controller. After heating was complete, the sample was passively cooled back to room temperature.

References

1. Ritchie, R. H. (1957). Plasma losses by fast electrons in thin films. *Phys. Rev.* **106**, 874–881
2. Burstein, E. (1974). Polaritons (Burstein, E. and De Martini, F., eds.). 1–4 Pergamon, New York
3. Kneipp, K., Wang, Y., Kneipp, H., Perelman, L. T., Itzkan, I., Dasari, R. R., and Feld, M. S. (1997). Single molecule detection using surface-enhanced Raman scattering (SERS). *Phys. Rev. Lett.* **78**, 1667–1670
4. Nie, S. M. and Emery, S. R. (1997). Probing single molecules and single nanoparticles by surface-enhanced Raman scattering. *Science.* **275**, 1102–1106
5. Ghindilis, A. L., Atanasov, P., Wilkins, M., and Wilkins, E. (1998). Immunosensors: Electrochemical sensing and other engineering approaches. *Biosens. Bioelectron.* **13**, 113–131
6. Chu, X., Lin, Z. H., Shen, G. L., and Yu, R. Q. M. (1995). Piezoelectric immunosensor for the detection of immunoglobulin M. *Analyst.* **120**, 2829–2832
7. Gauglitz, G. (1996). Opto-chemical and opto-immuno sensors, Sensor Update, Vol 1. VCH, Weinheim
8. Rowe-Taitt, C. A., Hazzard, J. W., Hoffman, K. E., Cras, J. J., Golden, J. P., and Ligler, F. S. (2000). Simultaneous detection of six biohaz ardous agents using a planar waveguide array biosensor. *Biosens. Bioelectron.* **15**, 579–589
9. Piehler, J., Brecht, A., and Gauglitz, G. (1996). Affinity detection of low molecular weight analytes. *Anal. Chem.* **68**, 139–143
10. Heideman, R. G., Kooyman, R. P. H., and Greve, J. (1993). Performance of a highly sensitive optical waveguide Mach-Zehnder interferometer immunosensor. *Sens. Actuators B* **10**, 209–217
11. Clerc, D. and Lukosz, W. (1994). Integrated optical output grating coupler as biochemical sensor. *Sens. Actuators B* **19**, 581–586
12. Cush, R., Cronin, J. M., Stewart, W. J., Maule, C. H., Molloy, J., and Goddard, N. J. (1993). The resonant mirror: a novel optical biosensor for direct sensing of biomolecular interactions part I: principle of operation and associated instrumentation. *Biosens. Bioelectron.* **8**, 347–353
13. Homola, J., Yee, S., and Gauglitz, G. (1999). Surface plasmon resonance sensors: review. *Sens. Actuators B* **54**, 3–15
14. Homola, J., Yee, S., and Myszka, D. (2002). Surface plasmon biosensors. In: Optical Biosensors: Present and Future (Ligler, F. S., and Taitt, C. R., eds.)., Elsevier, Amsterdam
15. Rabbany, S. Y., Lane, W. J., Marganski, W. A., Kusterbeck, A. W., and Ligler, F. S. (2000). Trace detection using a membrane-based displacement immunosassay. *J. Immunol. Methods* **246**, 69–77
16. Taton, T. A., Lu, G., Mirkin, C. A. (2001). Two-color labeling of oligonucleotide Arrays via size-selective scattering of nanoparticle probes. *J. Am. Chem. Soc.*, **123**, 5164–5165

17. El-Sayed, M. A. (2001). Some interesting properties of metals confined in time and nanometer space of different shapes. *Acc. Chem. Res.* **34**, 257–264
18. Jensen, T. R., Malinsky, M. D., Haynes, C. L., Van Duyne, R. P. (2000). Nanosphere lithography: tunable localized surface plasmon resonance spectra of silver nanoparticles. *J. Phys. Chem. B*, **104**, 10549
19. Schultz, S., Smith, D. R., Mock, J. J., Schultz, D. A. (2000). Single-target molecule detection with nonbleaching multicolor optical immunolabels. *Proc. Natl. Acad. Sci. U.S.A.*, **97**, 996
20. Michaels, A. M., Nirmal, M., Brus, L. E. (1999). Surface enhanced raman spectroscopy of individual rhodamine 6G molecules on large Ag nanocrystals. *J. Am. Chem. Soc.* **121**, 9932–9939
21. Yguerabide, J. and Yguerabide, E. E. (1998). Light-scattering submicroscopic particles as highly fluorescent analogs and their use as tracer labels in clinical and biological applications. *Anal. Biochem.* **262**, 157–176
22. Yguerabide, J. and Yguerabide, E. E. (1998). Light-scattering submicroscopic particles as highly fluorescent analogs and their use as tracer labels in clinical and biological applications. *Anal. Biochem.* **262**, 137–156
23. Schatz, G. C. and Van Duyne, R. P. (2002). Electromagnetic Mechanism of Surface-Enhanced Spectroscopy, Vol. 1. Wiley: New York
24. Kelly, K. L., Coronado, E., Zhao, L., and Schatz, G. C. (2003). The optical properties of metal nanoparticles: the influence of size, shape, and dielectric environment. *J. Phys. Chem. B*, **107**, 668–677
25. Kreibig, U., Gartz, M., and Hilger, A. (1997). Mie resonances. Sensors for physical and chemical cluster interface properties. *Ber. Bunsen-Ges.* **101**, 1593–1604
26. Link, S. and El-Sayed, M. A. (1999). Spectral properties and relaxation dynamics of surface plasmon electronic oscillations in gold and silver nanodots and vanorods. *J. Phys. Chem. B.* **103**, 8410–8426
27. Haynes, C. L. and Van Duyne, R. P.(2001). Nanosphere lithography: a versatile nanofabrication tool for studies of size-dependent nanoparticle optics. *J. Phys. Chem. B* **105**, 5599–5611
28. Mulvaney, P. (2001). Not all that's gold does glitter. *MRS Bull.* **26**, 1009–1014
29. Connolly, S., Cobbe, S., and Fitzmaurice, D. (2001). Effects of ligand-receptor geometry and stoichiometry on protein-induced aggregation of biotin-modified colloidal gold. *J. Phys. Chem. B.* **105**, 2222–2226
30. Storhoff, J. J., Lazarides, A. A., Mucic, R. C., Mirkin, C. A., Letsinger, R. L., and Schatz, G. C. (2000). What controls the optical properties of DNA-Linked gold nanoparticles assemblies. *J. Am. Chem. Soc.* **122**, 4640–4650
31. Henglein, A. and Meisel, D. (1998). Spectrophotometric observations of the adsorption of organosulfur compounds on colloidal silver nanoparticles. *J. Phys. Chem. B* **102**, 8364–8366
32. McFarland, A. D. and Van Duyne, R. P. (2003). Single silver nanoparticles as real-time optical sensors with zeptomole sensitivity. *Nano Lett.* **3**, 1057–1062
33. Malinsky, M. D., Kelly, K. L., Schatz, G. C., and Van Duyne, R. P. (2000). Chain length dependence and sensing capabilities of the localized surface plasmon resonance of silver nanoparticles chemically modified with alkanethiol self-assembled monolayers. *J. Am. Chem. Soc.* **123**, 1471–1482
34. Nath, N. and Chilkoti, A. (2002). A colorimetric gold nanoparticle sensor to interrogate biomolecular interactions in real time on a surface. *Anal. Chem.* **74**, 504–509
35. Riboh, J. C., Haes, A. J., McFarland, A. D., Yonzon, C. R., and Van Duyne, R. P. (2003). A nanoscale optical biosensor: real-time immunoassay in physiological buffer enabled by improved nanoparticle adhesion. *J. Phys. Chem. B* **107**, 1772–1780
36. Cao, Y. W., Jin, R. C., and Mirkin, C. A. (2002). Nanoparticles with Raman spectroscopic fingerprints for DNA and RNA Detection. *Science* **297**, 1536–1540
37. Calander, N. and Willander, M. (2002). Theory of surface-plasmon resonance optical-field enhancement at prolate spheroids. *J. Appl. Phys.* 92, 4878. Nils Calander, N. and Willander, M. (2002). Optical trapping of single fluorescent molecules at the detection spot of nanoprobes. *Phys. Rev. Lett.* **89**, 1436031–1436034
38. Sambles, J. R., Bradbery, G. W., and Yang, F. Z. (1991). Optical-excitation of surface-plasmons - an introduction. *Contemp. Phys.* **32**, 173–183
39. Boardman, A. D. (1982). Electromagnetic surface modes. Wiley, Chichester
40. Barnes, W. L., Dereux, A., and Ebbesen, T. W. (2003). Surface plasmon subwavelength optics. *Nature* **424**, 824–830
41. Kretschmann, E. and Raether, H. (1968). Radiative decay of nonradiative surface plasmons excited by light. *Z. Naturforsch. A* **23**, 2135–2136

42. Otto, A. (1968). Exitation of nonradiative surface plasma waves in silver by the method of frustrated total reflection. *Z. Phys.* **216**, 398
43. Hecht, B., Bielefeldt, H., Novotny, L., Inouye, Y., and Pohl, D. W. (1996). Local excitation, scattering, and interference of surface plasmons. *Phys. Rev. Lett.* **77**, 1889–1892
44. Ditlbacher, H., Krenn, J. R., Felidj, N., Lamprecht, B., Schider, G., Salerno, M., Leitner, A., and Aussenegg, F. R. (2002). Fluorescence imaging of surface plasmon fields. *Appl. Phys. Lett.* **80**, 404–406
45. Ritchie, R. H., Arakawa, E. T., Cowan, J. J.&Hamm, R. N. (1968). Surface-plasmon resonance effect in grating diffraction. *Phys. Rev. Lett.* **21**, 1530–1533
46. Raether, H. (1988). Surface Plasmons (Hohler, G., ed.)., Springer, Berlin
47. Ditlbacher, H., Krenn, J. R., Schider, G., Leitner, A., and Aussenegg, F. R. (2002). Two-dimensional optics with surface plasmon polaritons. *Appl. Phys. Lett.* **81**, 1762–1764
48. Cregan, R. F., Mangan, B. J., Knight, J. C., Birks, T. A., Russell, Roberts, P. J., and Allan, D. C. (1999). Single-mode photonic band gap guidance of light in air. *Science* **285**, 1537–1539
49. Kitson, S. C., Barnes, W. L., and Sambles, J. R. (1996). A full photonic band gap for surface modes in the visible. *Phys. Rev. Lett.* **77**, 2670–2673
50. Barnes, W. L., Preist, T. W., Kitson, S. C., and Sambles, J. R. (1996). Physical origin of photonic energy gaps in the propagation of surface plasmons on gratings. *Phys. Rev. B* **54**, 6227–6244
51. Barnes, W. L., Kitson, S. C., Preist, T. W., and Sambles, J. R. (1997). Photonic surfaces for surface plasmons polaritons. *J. Opt. Soc. Am. A* **14**, 1654–1661
52. Kreibig, U. and Vollmer, M. (1995). Optical properties of metal clusters. Springer, Berlin
53. Haynes, C. L. and Van Duyne, R. P. (2001). Nanosphere lithography: a versatile nanofabrication tool for studies of size-dependent nanoparticle optics. *J. Phys. Chem. B* **105**, 5599–5611
54. Sonnichsen, C., Geier, S., Hecker, N. E., von Plessen, G., Feldmann, J., Ditlbacher, H., Lamprecht, B., Krenn, J. R., Aussenegg, F. R., Chan, V. Z.-H., Spatz, J. P., and Moller, M. (2000). Spectroscopy of single metallic nanoparticles using total internal reflection microscopy. *Appl. Phys. Lett.* **77**, 2949–2951
55. Schultz, D. A. (2003). Plasmon resonant particles for biological detection. *Curr. Opin. Biotechnol.* **14**, 13–22
56. Oldenburg, S. J., Genick, C. C., Clark, K. A., and Schultz, D. A. (2002). Base pair mismatch recognition using plasmon resonant particle labels. *Anal. Biochem.* **309**, 109–116
57. Félidj, N., Aubard, J., Levi, G., Krenn, J. R., Hohenau, A., Schider, G., Leitner, A., and Aussenegg, F. R. (2003). Optimized surface-enhanced Raman scattering on gold nanoparticle arrays. *Appl. Phys. Lett.* **82**, 3095–3097
58. Levi, S., Mourran, A., Spatz, J. P., Veggel van, F., Reinhoudt, D., and Moller, M. (2002). Fluorescence of dyes adsorbed on highly organized, nanostructured gold surfaces. *Chem. Eur. J.* **8**, 3808–3814
59. Vargas-Baca, I., Brown, A. P., Andrews, M. P., Galstian, T., Li, Y., Vali, H., and Kuzyk, M. G. (2002). Linear and nonlinear optical responses of a dye anchored to gold nanoparticles dispersed in liquid and polymeric matrixes. *Can. J. Chem.* **80**, 1625–1633
60. Rechberger, W., Hohenau, A., Leitner, A., Krenn, J. R., Lamprecht, B., and Aussenegg, F. R. (2003). Optical properties of two interacting gold nanoparticles. *Opt. Commun.* **220**, 137–141
61. Kottmann, J. P. and Martin, O. J. F. (2001). Retardation-induced plasmon resonances in coupled nanoparticles. *Opt. Lett.* **26**, 1096–1098
62. García-Vidal, F. J. and Pendry, J. B. (1996). Collective theory for surface enhanced Raman scattering. *Phys. Rev. Lett.* **77**, 1163–1166
63. Gresillon, S., Aigouy, L., Boccara, A. C., Rivoal, J. C., Quelin, X., Desmarest, C., Gadenne, P., Shubin, V. A., Sarychev, A. K., and Shalaev, V. M. (1999). Experimental observation of localized optical excitations in random metal-dielectric films. *Phys. Rev. Lett.* **82**, 4520–4523
64. Homola, J. (2003). Present and future of surface plasmon resonance biosensors. *Anal. Bioanal. Chem.* **377**, 528–539
65. Snyder, A. W. and Love, J. D. (1983). Optical waveguide theory. Chapman and Hall, London
66. Parriaux, O. and Voirin, G. (1990). Plasmon wave versus dielectric waveguiding for surface wave sensing. *Sens. Actuators A* **23**, 1137–1141
67. Reather, H. (1983). Surface Plasmons on Smooth and Rough Surfaces and on Gratings, Springer Tracts in Modern Physics, Vol. 111, Springer, Berlin
68. Nylander, C., Liedberg, B., and Lind, T. (1982). Gas detection by means of surface plasmons resonance. *Sens. Actuators* **3**, 79–88

69. Liedberg, B., Nylander, C., and Lundstro¨m, I. (1983). Surface plasmons resonance for gas detection and biosensing. *Sens. Actuators* **4**, 299–304
70. Matsubara, K., Kawata, S., and Minami, S. (1988). Optical chemical sensor based on surface plasmon measurement. *Appl. Opt.* **27**, 1160–1163
71. Liedberg, B., Lundstrom, I., and Stenberg, E. (1993). Principles of biosensing with an extended coupling matrix and surface plasmon resonance. *Sens. Actuators B* **11**, 63–72
72. Zhang, L. M. and Uttamchandani, D. (1988). Optical chemical sensing employing surface plasmon resonance. *Electron. Lett.* **23**, 1469–1470
73. Jonsson, U., Fagerstam, L., Ivarsson, B., Johnsson, B., Karlsson, R., Lundh, K., Lofas, S., Persson, B., Roos, H., Rönnberg, I., et al. (1991). Real-time biospecific interaction analysis using surface plasmon resonance and a sensor chip technology. *Biotechniques* **11**, 620–627
74. Löfås, S., Malmqvist, M., Rönnberg, I., Stenberg, E., Liedberg, B., and Lundström, I. (1991). Bioanalysis with surface plasmon resonance. *Sens. Actuators B* **5**, 79–84
75. Hutley, M. C. (1982). Diffration gratings. Academic Press, London
76. Hutley, M. C. (1982). Diffration gratings, Academic Press, London
77. Raether, H. (1988). Surface Plasmons on Smooth and Rough Surfaces and on Gratings. Springer-Verlag, Berlin
78. Moharam, M. G. and Gaylord, T. K. (1986). Rigorous coupled-wave analysis of metallic surface-relief gratings. *J. Opt. Soc. Am A.* **3**, 1780–1787
79. Chandezon, J., Dupuis, M. T., Cornet, G., and Maystre, D. (1982). Multicoated gratings: a differential formalism applicable an the entire optical region. *J. Opt. Soc. Am.* **72**, 839–846
80. Cullen, D. C., Brown, R. G., and Lowe, C. R. (1987). Detection of immunocomplex formation via surface plasmon resonance on goldcoated diffraction gratings. *Biosensors* **3**, 211–225
81. Cullen, D. C. and Lowe, C. R. (1990). A direct surface plasmon-polariton immunosensor: preliminary investigation of the nonspecific adsorption of serum components to the sensor interface. *Sens. Actuators B* **1**, 576–579
82. Vukusic, P. S., Bryan-Brown, G. P., and Sambles, J. R. (1992). Surface plasmons resonance on grating as novel means for gas sensing. *Sens. Actuators B* **8**, 155–160
83. Jory, M. J., Vukusic, P. S., and Sambles, J. R. (1994). Development of a prototype gas sensor using surface plasmon resonance on gratings. *Sens. Actuators B* **17**, 1203–1209
84. Jorgenson, R. C. and Yee, S. S. (1993). A fiber-optic chemical sensor based on surface plasmon resonance. *Sens. Actuators B* **12**, 213–220
85. Jorgenson, R. C. and Yee, S. S. (1994). Control of the dynamic range and sensitivity of a surface plasmon resonance based fiber optic sensor. *Sens. Actuators A* **43**, 44–48
86. Trouillet, A., Ronot-Trioli, C., Veillas, C., and Gagnaire, H. (1996). Chemical sensing by surface plasmon resonance in a multimode optical fibre. *Pure Appl. Opt.* **5**, 227–237
87. Ronot-Trioli, C., Trouillet, A., Veillas, C., and Gagnaire, H. (1996). Monochromatic excitation of surface plasmon resonance in an optical-fibre refractive-index sensor. *Sens. Actuators A* **54**, 589–593
88. Dessy, R. E. and Bender, W. J. (1994). Feasibility of a chemical microsensor based on surface plasmon resonance on fiber optics modified by multilayer vapor deposition. *Anal. Chem.* **66**, 963–970
89. Homola, J. (1995). Optical fiber sensor based on surface plasmon excitation, Second European Conference on Optical Chemical Sensors and Biosensors, Florence, Italy, April 1994. *Sens. Actuators B* **29**, 401–405
90. Homola, J. and Slavik, R. (1996). Fibre-optic sensor based on surface plasmon resonance. *Electron. Lett.* **32**, 480–482
91. Tubb, A. J. C., Payne, F. P., and Millington, R. B. (1997). C. R. Lowe, Singlemode optical fiber surface plasma wave chemical sensor. *Sens. Actuators B* **41**, 71–79
92. Homola, J., Tyroky, J. C., Skalsky, M., Hradilova, J., and Kola´r' ova´P. (1997). A surface plasmon resonance based integrated optical sensor. *Sens. Actuators B* 38–39, 286–290
93. Lavers, C. R. and Wilkinson, J. S. (1994). A waveguide-coupled surface plasmon sensor for an aqueous environment. *Sens. Actuators B* **22**, 75–81
94. Harris, R. D. and Wilkinson, J. S. (1995). Waveguide surface plasmon resonance sensors. *Sens. Actuators B* **29**, 261–267
95. Mouvet, C., Harris, R. D., Maciag, C., Luff, B. J., Wilkinson, J. S., Piehler, J., Brecht, A., Gauglitz, G., Abuknesha, R., and Ismail, G. (1997). Determination of simazine in water samples by waveguide surface plasmon resonance. *Anal. Chim. Acta* **338**, 109–117

96. Ctyroky, J., Homola, J., and Skalsky, M. (1997). Tuning of spectral operation range of a waveguide surface plasmon resonance sensor. *Electron. Lett.* **33**, 1246–1248
97. Weiss, M. N., Srivastava, R., Groger, H., Lo, P., and Luo, S. F. (1996). A theoretical investigation of environmental monitoring using surface plasmon resonance waveguide sensors. *Sens. Actuators A* **51**, 211–217
98. Weiss, M. N., Srivastava, R., and Groger, H. (1996). Experimental investigation of a surface plasmon-based integrated-optic humidity sensor. *Electron. Lett.* **32**, 842–843
99. Bender, W. J. H., Dessy, R. E., Miller, M. S., and Claus, R. O. (1994). Feasibility of a chemical microsensor based on surface plasmon resonance of fiber optics modified by multilayer vapor deposition. *Anal. Chem.* **66**, 963–970
100. Kooyman, R. P. H., Kolkman, H., van Gent, J., and Greve, J. (1988). Surface plasmon resonance immunosensors: sensitivity considerations. *Anal. Chim. Acta* **213,** 35–45
101. Yeatman, E. M. (1996). Resolution and sensitivity in surface plasmon microscopy and sensing. *Biosens. Bioelectron.* **11**, 635–649
102. Homola, J. (1997). On the sensitivity of surface-plasmon resonance sensors with spectral interrogation. *Sens. Actuators B* **41**, 207–211
103. Homola, J., Koudela, I., and Yee, S. (1999). Surface plasmon resonance sensors based on diffraction gratings and prism couplers: sensitivity comparison. *Sens. Actuators B* **54**, 16–24
104. Edwards, P. R. and Leatherbarrow, R. J. (1997). Determination of association rate constants by an optical biosensor using initial rate analysis. *Anal. Biochem.* **246,** 1–6
105. Vijayendran, R. A., Ligler, F. S., and Leckband, D. E. (1999). A computational reaction-diffusion model for the analysis of transport limited kinetics. *Anal. Chem.***71**, 5405–5412
106. Rich, R. L. and Myszka, D. G. (2002). Survey of the year 2001 commercial optical biosensor literature. *J. Mol. Recognit.* **15,** 352–376
107. Severs, A. H. and Schasfoort, R. B. M. (1993). Enhanced surface plasmon resonance inhibition test (ESPRIT). using latex particles. *Biosens. Bioelectron.* 8, 365–370
108. Leung, P. T., Pollard-Knight, D., Malan, G. P., and Finlan, M. F. (1994). Modelling of particle-enhanced sensitivity of the surface-plasmon-resonance biosensor. *Sens. Actuators B* **22,** 175–180
109. Owen, V. (1997). Real-time optical immunosensors – a commercial reality, *Biosens. Bioelectron.* **12,** i–ii
110. Berger, C. E. H., Baumer, T. A. M., Kooyman, R. P. H., and Greve, J. (1998). Surface plasmon resonance multisensing. *Anal. Chem.* **70,** 703–706